CCFE
CULHAM CENTRE FOR FUSION ENERGY

UK Atomic Energy Authority

UKAEA-CCFE-PR(21)09

B. C. G. Reman, R. O. Dendy, T. Akiyama, S. C. Chapman, J. W. S. Cook, H. Igami, S. Inagaki, K. Saito, M.H. Kim, S.G. Thatipamula, G. S. Yun

Density dependence of ion cyclotron emission from deuterium plasmas in the Large Helical Device

Density dependence of ion cyclotron emission from deuterium plasmas in the Large Helical Device

B. C. G. Reman, R. O. Dendy, T. Akiyama, S. C. Chapman, J. W. S. Cook, H. Igami, S. Inagaki, K. Saito, M.H. Kim, S.G. Thatipamula, G. S. Yun

This is a preprint of a paper submitted for publication in Nuclear Fusion

Density dependence of ion cyclotron emission from deuterium plasmas in the Large Helical Device

B. C. G. Reman*[1], R. O. Dendy[2,1], T. Akiyama †[3], S. C. Chapman[1], J. W. S. Cook[2,1], H. Igami[3], S. Inagaki[4], K. Saito[3], M.H. Kim[5], S.G. Thatipamula[5], and G. S. Yun[5]

[1]Centre for Fusion, Space and Astrophysics, Department of Physics, Warwick University, Coventry CV4 7AL, UK

[2]CCFE, Culham Science Centre, Abingdon, Oxfordshire OX14 3DB, UK

[3]National Institute for Fusion Science, Toki, Gifu 509-5292, Japan

[4]Research Institute for Applied Mechanics, Kyushu University, Kasuga 816-8580, Japan

[5]Department of Physics, Pohang University of Science and

Technology, Pohang 37673, Korea

Abstract

Ion cyclotron emission (ICE) driven by perpendicular neutral beam-injected (NBI) deuterons, together with the distinctive ICE driven by tangential NBI, have been observed from heliotron-stellarator plasmas in the Large Helical Device (LHD). Radio frequency radiation in the lower hybrid range has also been observed [1], with frequency dependent on plasma density. Here we focus on recent measurements of ICE from deuterium plasmas in LHD, which show substantial variation in spectral character, between otherwise similar plasmas that have different local density in the emitting region. Here we analyse this variation by means of first principles simulations, carried out using a particle-in-cell (PIC) kinetic approach. We show, first, that this ICE is driven by perpendicular NBI deuterons, freshly ionised near their injection point in the outer midplane edge of LHD. We find that these NBI deuterons undergo collective sub-Alfvénic relaxation, which we follow deep into the nonlinear phase of the magnetoacoustic cyclotron instability. The frequency and wavenumber dependence of the saturated amplitudes of the excited fields determine our simulated ICE spectra, and these spectra are obtained for different local densities corresponding to the different LHD ICE-emitting plasmas.

*Now at Laboratoire Plasma et Conversion d'Energie, Université Toulouse III Paul-Sabatier, France

†Now at General Atomics, P.O. Box 85608, San Diego, CA 92186, USA

The variation with density of the spectral character of the simulated ICE corresponds well with that of the observed ICE from LHD. These results from heliotron-stellarator plasmas complement recent studies of density-dependent ICE from tokamak plasmas in KSTAR [2, 3], where the spectra vary on sub-microsecond timescales after an ELM crash. Taken together, these results confirm the strongly spatially localised character of ICE physics, and reinforce the potential of ICE as a diagnostic of energetic ion populations and of the ambient plasma.

1 Introduction

Ion cyclotron emission (ICE) is widely observed from magnetically confined fusion (MCF) plasmas [4]. In addition to historical observations from deuterium-tritium plasmas in JET [5, 6] and TFTR [7], since 2017 ICE has been reported and analysed from the KSTAR [8, 9], DIII-D [10], ASDEX-Upgrade [11, 12, 13], Tuman-3M [14] and EAST [15] tokamaks, and the LHD heliotron-stellarator [16, 17, 18]. ICE spectra typically comprise a succession of narrow, strongly suprathermal, peaks at sequential cyclotron harmonics of an energetic ion species. These species include fusion-born ions [5], neutral beam injected (NBI) ions [19], and ions energised by ion cyclotron resonant heating (ICRH) [20]. The emitting region is identified by matching spectral peak frequencies to local magnetic field strength. While in most cases it corresponds to the outer midplane edge plasma, ICE from the plasma core has recently been reported from the ASDEX-Upgrade [12] and DIII-D [21]

tokamaks. It is clear that the plasma physics process responsible for ICE is the magnetoacoustic cyclotron instability (MCI) [22]. This excites waves on the fast Alfvén-cyclotron harmonic branch, by drawing on the free energy of fast ions whose distribution in velocity-space incorporates a population inversion. The linkage between ICE and the MCI was established by early analytical studies [23, 24, 25, 26], and reinforced in the past decade by first principles computational studies using the particle-in-cell (PIC) approach [27, 28, 29, 30, 20, 3, 8, 9].

PIC code algorithms [31] solve the Maxwell-Lorentz system of equations, typically for tens or hundreds of millions of interacting charged particles - energetic ions, thermal ions, and electrons - together with the self-consistent electric and magnetic fields. Collective instabilities thus emerge at the level of particle kinetics and field dynamics. The PIC approach can retain full gyro-orbit resolution, and is thus particularly suitable for phenomena that incorporate gyroresonance, such as the MCI. In PIC studies for ICE interpretation, a minority energetic ion population is initialised with a distinct, physically motivated, velocity-space inversion. This population then relaxes under the Maxwell-Lorentz system, while coupled to the thermal ions and electrons, and interacting with, and generating, self-consistent fields. Typically, the frequency and wavenumber dependence of the saturated amplitudes of the MCI-excited fields determine the simulated ICE spectra, which are then compared to the observed ICE spectra.

The foregoing approach was recently applied to observations of ICE from hydrogen plasmas in LHD, driven by NBI protons injected perpendicular to

the confining magnetic field [18]. A focus of Ref. [18] is the dependence of observed ICE properties on whether the NBI protons are super-Alfvénic or sub-Alfvénic in the emitting region of the plasma; that is, whether v_{NBI}/V_A is larger or smaller than unity, where v_{NBI} is the speed of the NBI ions and V_A the local Alfvén speed. The present computational study addresses measurements of ICE from significantly sub-Alfvénic populations of energetic NBI ions, under conditions where the local density differs significantly between LHD plasmas. At fixed NBI energy and local field strength, the value of V_A is governed by the value of the density. In recent PIC studies of ICE from the KSTAR tokamak, ICE chirping on sub-microsecond timescales during the ELM crash was interpreted [3] in terms of fast density dependence arising from filament motion. Understanding the density dependence of ICE phenomenology is thus topical, both experimentally and in relation to theory and interpretation. In particular, it will assist the exploitation of ICE measurements to infer the key features of the velocity-space distribution of energetic ion populations in MCF plasmas.

In the LHD heliotron-stellarator, the ICE driven by perpendicular NBI deuterium, and the distinctive ICE driven by tangential NBI, have previously been observed using loop antennas [1]. Moreover, radiofrequency emission has been observed in the lower hybrid range, with frequency dependent on plasma density. Here we address recent measurements of radio-frequency emission at multiple deuteron cyclotron harmonics from deuterium plasmas in LHD, which show substantial variation in spectral character, between otherwise similar plasmas that have different local density in the emitting

region. These measurements are obtained with the dipole antenna described below. We show that this ICE is driven by perpendicular NBI deuterons, freshly ionised near their injection point in the outer midplane edge of LHD. These NBI deuterons undergo collective sub-Alfvénic relaxation, which we follow deep into the nonlinear phase of the magnetoacoustic cyclotron instability. The variation with density of the spectral character of the simulated ICE corresponds well with that of the observed ICE from LHD. These results from heliotron-stellarator plasmas complement recent studies of density-dependent ICE from tokamak plasmas in KSTAR [2, 3], where the spectra vary on sub-microsecond timescales after an ELM crash. Taken together, these results confirm the strongly spatially localised character of ICE physics, and reinforce the potential of ICE as a diagnostic of energetic ion populations and of the ambient plasma.

Our PIC computational approach, using the hybrid-PIC code [28], is the same as used in Ref.[18], to which we refer for further detail.

On LHD, the acquisition system of the ICE measured at a dipole antenna located in the 10-O port inside the vacuum vessel was developed in partnership with KSTAR [32, 33, 34, 35]. A fast digitizer performs direct sampling of the radiofrequency measurements at a frequency of 1.25GSa/s. The time evolution of the RF spectral intensity is determined from this signal using a 14-channel filter bank spectrometer in the range of 70MHz to 2800 MHz, with intermediate spectral resolution and with μs time resolution; for a duration spanning the whole plasma discharge [34]. This dipole antenna measuring the ICE is located close to NBI #5 and toroidally opposite to

NBI #4, see Fig. 4.

2 Observed density dependence of ICE during perpendicular deuterium NBI

During perpendicular deuterium NBI experiments in LHD, it was observed that the spectral character of the ICE changes significantly between plasmas whose parameters in the emitting edge region differ only in their electron density. The left panel of figure 1 shows that ICE at frequencies 30MHz and 60MHz was observed only when NBI # 5 was operated without NBI #4 in LHD plasmas 138439 and 138458. Conversely, in these plasmas, ICE was not observed when only NBI #4 was operated without NBI #5. Moreover, as shown in the right panel of Fig. 1, ICE was continuously observed during continuous operation of NBI #5 in LHD plasma 138433. These results support the interpretation below that ICE measured at the dipole antenna is driven locally by perpendicular-NB injected deuterons from NBI #5. Figure 2 shows the ICE power spectra observed at the time indicated by the vertical blue dashed line in Fig. 1 for LHD plasmas 138439, 138458 and 138433 which differ primarily in their edge plasma densities. The profiles of the electron density, electron temperature, and ion temperature are shown in Fig. 3. These were taken at instants which are very close to the times at which the ICE spectra, shown in Fig. 2, were observed. Figure 2 shows that, as the electron density increases, the amplitudes of the ICE spectral peaks typically

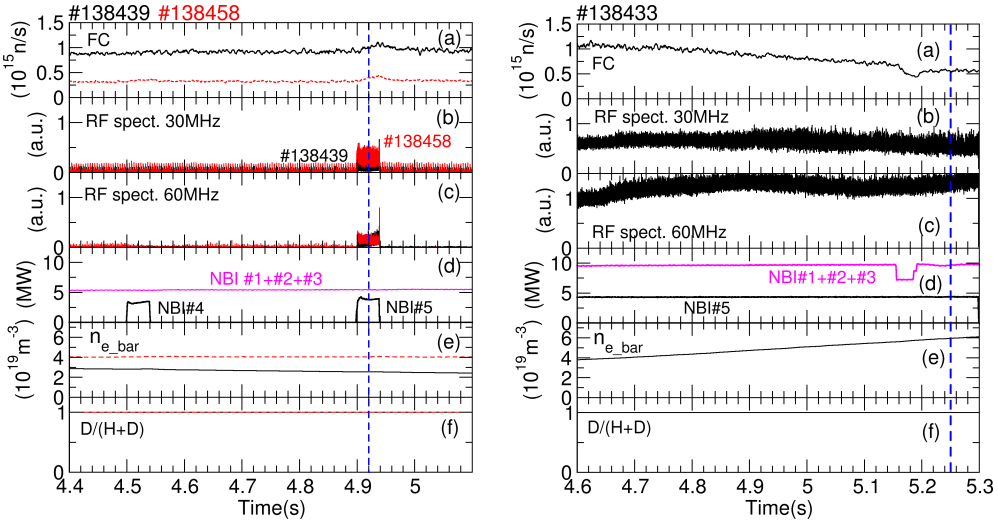

Figure 1: Measured time traces for: (left panel) LHD plasmas 138439 (black traces) and 138458 (red), to which NBI #4 and NBI #5 were applied in separate brief bursts; (right panel) LHD plasma 138433 during which NBI # 5 was operated continuously. From top to bottom, the six vertically arranged panels are: (a) neutron flux; emission intensity detected by RF spectrometer for frequency channels at (b) 30MHz and (c) 60 MHz; (d) NBI port through power; (e) line averaged density; and (f) the ratio of the number deuterons to the total number of hydrogenic ions, which is close to unity.

increase, in the frequency range of interest to us below 120 MHZ; the number of harmonics increases; and the width of spectral peaks increases.

If we identify the 12.05MHz spacing between the ICE spectral peaks in Fig. 2 with the local deuterium cyclotron frequency, this suggests that the local background magnetic field value is 1.581T and hence the emission location is at $R = 4.651$m, as illustrated in Fig. 5. Table 1 summarises the plasma parameters at the inferred emission location where the deuteron cyclotron frequency matches 12.05 MHz, with reference to Fig. 3, together with values for the velocity of freshly injected ions v_{NBI}, and the local Alfvén speed V_A.

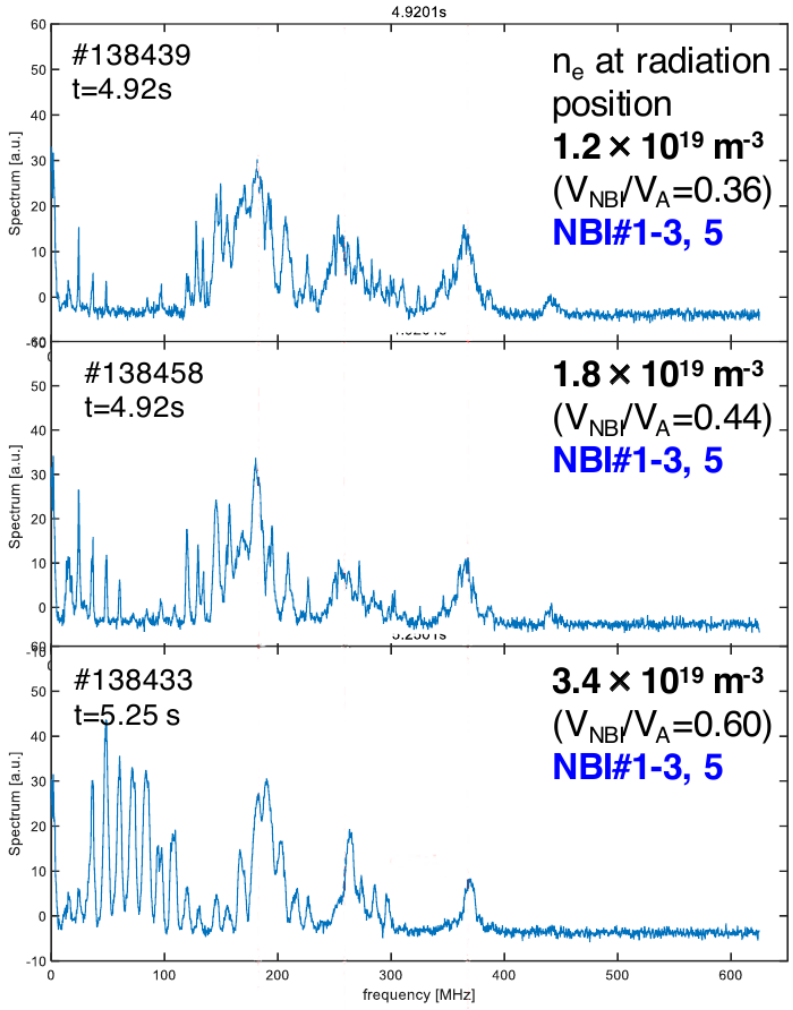

Figure 2: Observed ICE power spectra for three LHD plasmas at times indicated by the blue vertical dashed lines in Fig. 1 for LHD plasmas 138439, 138458 and 138433 which differ primarily in their edge plasma densities. The peak-to-peak frequency separation Δf is equal to 12.05MHz in all three cases. Identifying Δf with the local deuteron cyclotron frequency Ω_D implies a magnetic field strength $B = 1.581$T, and this corresponds to an outer midplane edge location in LHD.

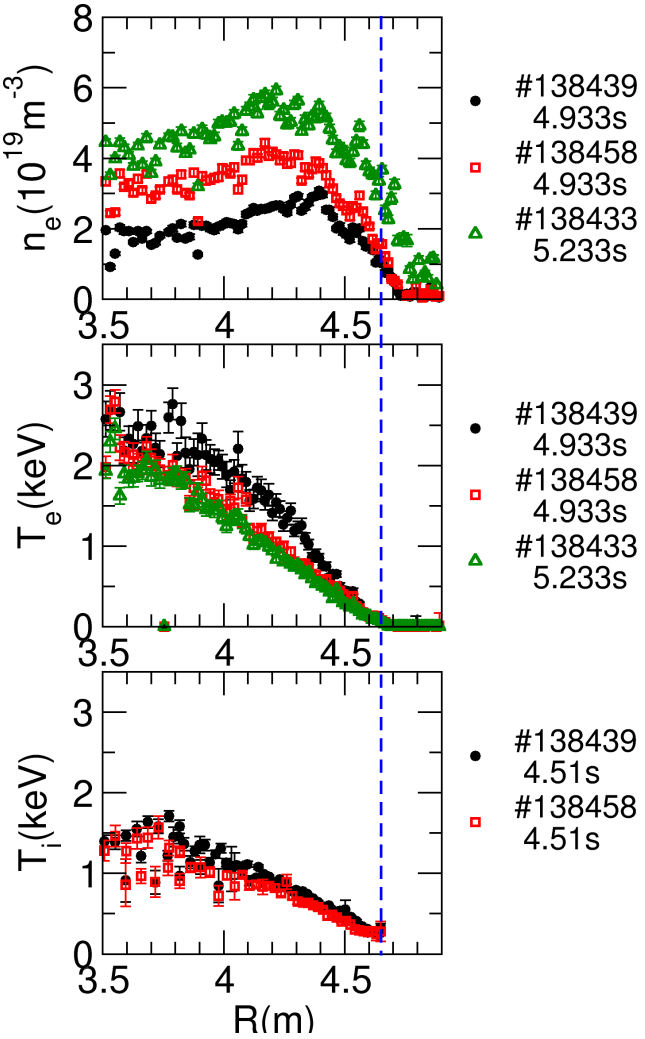

Figure 3: Measured radial profiles of the LHD plasmas. (Top) electron density, and (middle) electron temperature, obtained by Thomson scattering at the time of the ICE spectra displayed in Fig. 1; (bottom) ion temperature obtained by charge exchange spectroscopy during heating by NBI # 4.

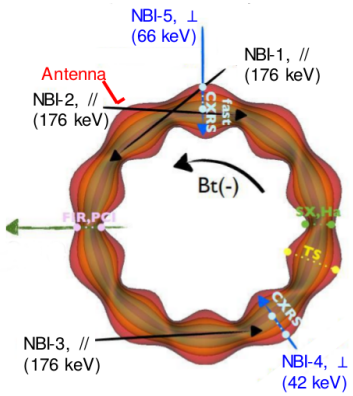

Figure 4: Schematic diagram of LHD plasma showing locations and directions of NBI beams.

We note for future analysis that, since the Alfvén speed is given by

$$V_A = \frac{B_0}{\sqrt{\mu_0 n_e m_D}} \tag{1}$$

with n_e and m_D the electron density and the deuteron mass respectively, the key dimensionless ratio of the NBI deuteron speed to the Alfvén speed, v_{NBI}/V_A, also increases as n_e increases. We observe that in all three plasmas, the NBI deuterons are in the sub-Alfvénic regime. This regime was previously investigated in earlier ICE experiments carried out in TFTR, involving gas puffing [36, 37]. This changed the edge plasma density, transitioning the fusion-born alpha-particles from a sub-Alfvénic to a super-Alfvénic regime in that region. The consequences for the TFTR ICE spectrum are discussed in Figs. 7 to 9 of Ref. [37].

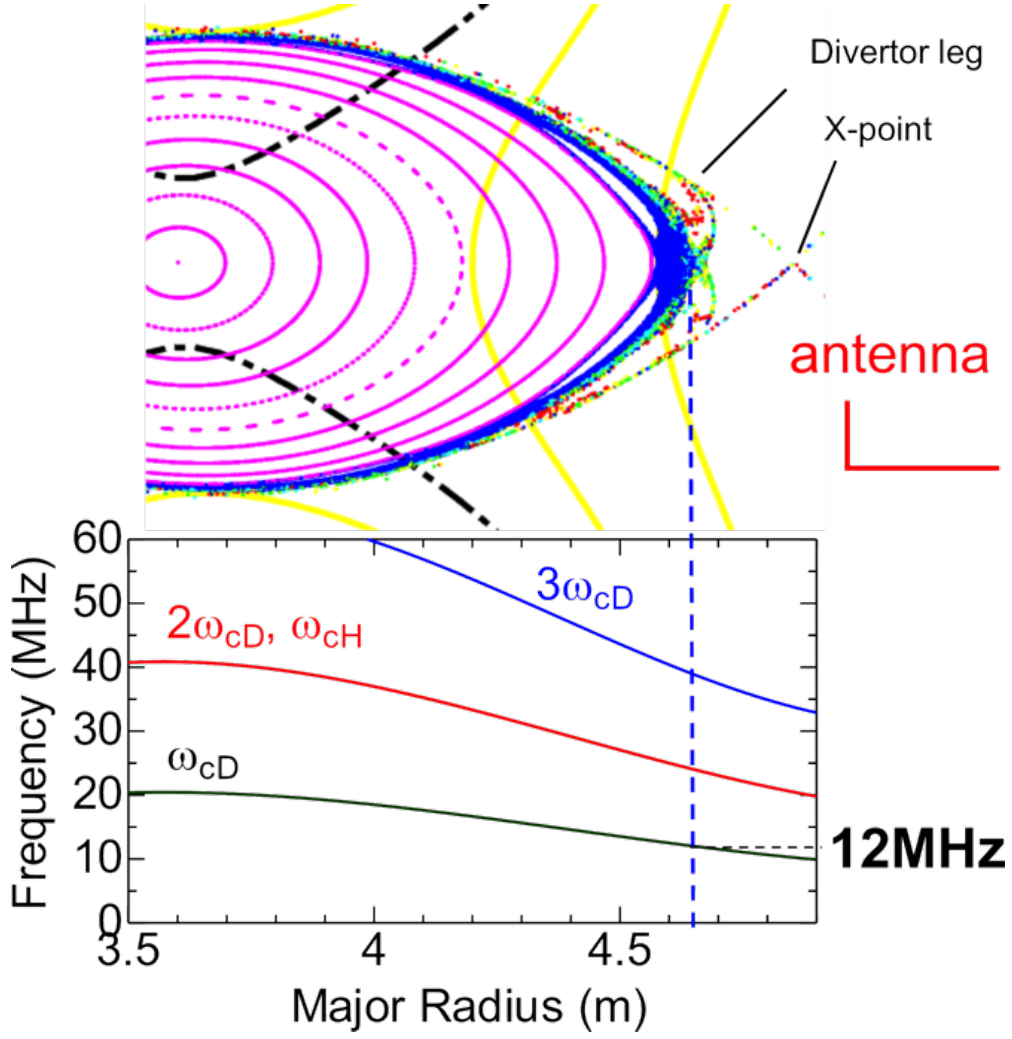

Figure 5: Identifying the approximate location of the region where ICE is generated during perpendicular deuterium NBI in LHD. We match the approximate frequency spacing between observed neighbouring ICE peaks, $\simeq 12$ MHz, to the spacing between successive local deuteron cyclotron harmonics. This is possible only at $R \simeq 4.65$m.

LHD plasma	T_e (eV)	n_e $10^{19}\mathrm{m}^{-3}$	NBI #5b keV	v_{NBI} $10^6\mathrm{ms}^{-1}$	V_A $10^6\mathrm{ms}^{-1}$	v_{NBI}/V_A
138439	70	1.2	66.7	2.53	7.04	0.36
138458	80	1.8	66.7	2.53	5.75	0.44
138433	50	3.4	68.7	2.57	4.18	0.61

Table 1: Edge plasma parameters and NBI deuteron energies, with corresponding values for v_{NBI}/V_A which are significantly sub-Alfvénic.

LHD plasma	NBI#1 (keV),D	NBI#2 (keV),H	NBI#3 (keV), D	NBI#4a (keV), D	NBI#4b (keV), D	NBI#5a (keV), D	NBI#5b (keV), D
138439	172	-	174	30.5	45.2	-	66.7
138458	172	138	-	30.5	46.2	-	66.7
138433	172	163	174	35.4	51.1	-	68.7

Table 2: Table giving the different NBI energies, either H or D. The simulations use the deuterium energies of NBI #5b. Note from Fig. 4 that NBI #1, #2 and #3 are all directed parallel, whereas NBI #4 and #5 are perpendicular to the magnetic field.

3 First principles simulations of ICE spectra and their density dependence

3.1 Basis of the computational approach

Our hybrid-PIC simulations, reported below, use the deuterium injection energies of NBI #5*b* given in Table 2 to define the initial perpendicular velocity of the energetic minority deuteron population. These deuterons are represented in velocity space as a gyro-resolved ring-beam distribution $\sim \delta\left(v_{\perp} - v_{NBI}\right)$, as discussed further in Sec. 3.2, which coexists with a much more numerous gyro-resolved thermal deuteron population together with a charge-neutralising electron fluid. Once initialised, this system subsequently relaxes under first principles self-consistent Maxwell-Lorentz dynamics. The majority thermal deuterons have $T_i = 280$eV, which is inferred from the LHD ion temperature profile shown in Fig. 3 in combination with the result of Fig 5; we use the associated thermal velocity $v_{Ti} = 1.64 \times 10^5$ ms^{-1} to characterise their initially Maxwellian distribution. It follows that $v_{NBI}/v_{Ti} = 15.43$, which is also the ratio of ion Larmor radii $r_{L,NBI}/r_{Ti}$. We use 32798 particles per cell for the thermal background deuterons and 8192 particles per cell for the NBI deuterons. The 1.581T background magnetic field is perpendicular to the 1D spatial domain of our simulation, which consists of 4096 cells. The cell sizes are 0.0028m, 0.0022m and 0.0014m for LHD plasma 138439, 138458 and 138433 respectively, which correspond respectively to multiples of 1.31, 1.00 and 0.65 of the characteristic gyro-

radius r_{Ti} of the thermal deuterons. The different plasma densities give rise to different electron skin depths λ_e: 0.0015m, 0.0013m and 0.0009m, respectively. These need to be smaller than the cell sizes to be consistent with PIC-hybrid model assumptions [38, 39]. Chosen as above, the cell sizes keep the ratio of $\Delta x/\lambda_e$ constant at about 1.70 in all three cases. This approach thus captures cyclotron resonant phenomenology directly, at the level of particle-field interactions for individual ions moving on their resolved gyro-orbits. To enable systematic comparison of computational outputs, we use the same relative beam density $\xi \equiv n_{NBI}/n_e$ for all our simulations; as distinct from, say, a constant absolute beam density. Specifically, we set $\xi = 0.0005$ in all simulations.

The ratios of the NBI deuteron speed v_{NBI} to the local Alfvén speed V_A are 0.36, 0.44 and 0.60 for LHD plasmas 138439, 138458 and 138433 respectively, see Table 1. The NBI deuterons are thus in a significantly sub-Alfvénic (and accordingly computationally resource-intensive) regime for all three plasmas; they have an even lower value of v_{NBI}/V_A than the sub-Alfvénic NBI protons in LHD hydrogen plasmas whose ICE was addressed in Ref. [18].

3.2 Simulated ICE spectra compared to observations

In our PIC-hybrid simulations, the energetic minority deuteron population is initialised with a ring-beam distribution in velocity space, of the form $f_{NBI}\left(v_\perp, v_\parallel\right) = 1/\left(2\pi v_{NBI}\right)\delta\left(v_\parallel\right)\delta\left(v_\perp - v_{NBI}\right)$, where v_{NBI} the injection speed resulting from the NBI #5b beam energies given in Table 1. These

NBI deuterons are initially distributed randomly and uniformly in gyroangle while the thermal deuterons are loaded by mean of a quiet start [40, 41], in both positions and velocities. The relaxation of this energetic ion population under the Maxwell-Lorentz system of equations gives rise to self-consistently excited electric and magnetic fields; see Refs. [27, 28, 3] for details of this approach. Fourier transformation of the excited fields yields spectral information that is compared to the LHD observations. We focus on the lower cyclotron harmonics, for which the distribution of energy between the ICE spectral peaks shown in Fig. 2 displays significant changes between the three LHD plasmas. Figure 6 shows the simulated power spectra, alongside the measured spectra extracted from Fig. 2. The red, green and blue traces correspond to LHD plasmas 138439, 138458 and 138433 respectively. In the middle and bottom panels of Fig. 6, these traces are obtained by taking the spatiotemporal fast Fourier transform of the values of δB_z output from the PIC-hybrid computations in the time interval between $t = \tau_D$ and $t = 9\tau_D$ (where $\tau_D = 2\pi/\Omega_D$), which is summed over wavenumbers up to $k = 40\Omega_D/V_A$. The agreement between observed and simulated ICE spectra appears good quantitatively. In both the top (experimental ICE) and middle (simulated spectra) panels in Fig. 6, the number of cyclotron harmonic spectral peaks increases as v_{NBI}/V_A increases, as does their amplitude. These trends can be examined in greater detail for the three plasmas separately in Fig. 7. Here our simulated power spectra are shown as dark traces, together with the measured ICE spectra which are plotted as coloured traces for comparison: red, LHD plasma 138439; green, LHD plasma 138458; blue, LHD

plasma 138433. The spectra are vertically offset in comparison with Fig. 6 such that the ordinate of the peak with largest amplitude is zero in each panel. In the left panel of Fig. 7, for which $v_{NBI}/V_A = 0.36$, the strongest spectral peaks in the simulation are at relatively low deuteron cyclotron harmonics, second to fourth. In the middle panel, for which $v_{NBI}/V_A = 0.44$, the middle order harmonics (fourth and fifth) become more pronounced. In the right panel of Fig. 7, for which $v_{NBI}/V_A = 0.60$, the amplitudes of the spectral peaks are substantially larger, and the simulation captures the experimental spectrum in extending strongly across the middle order harmonics (fifth to seven). In all three plasmas of Fig. 7, the strongest harmonic peaks in the experiment and in the simulations are the same: from left, second, second and fourth.

The fundamental computational noise level in our simulations is addressed in Appendix A, where it is found to lie at about -145dB. The instrumental noise level in the ICE detection system on LHD imposes the noise floor that is visible in the top panel of Fig. 6. The question of where the instrumental noise floor should lie in our simulated spectra cannot be answered *a priori*. However the bottom panel of Fig. 6 shows that the agreement between the observed and simulated ICE spectra is greatest if we conjecturally assign a value of -133dB to the instrumental noise floor when considering our simulated spectra.

The spatiotemporal fast Fourier transforms of δB_z are plotted in Fig. 8. These show that the concentration of excited wave amplitude in (ω, k) space lies on horizontal bands at successive cyclotron harmonics, and that each of

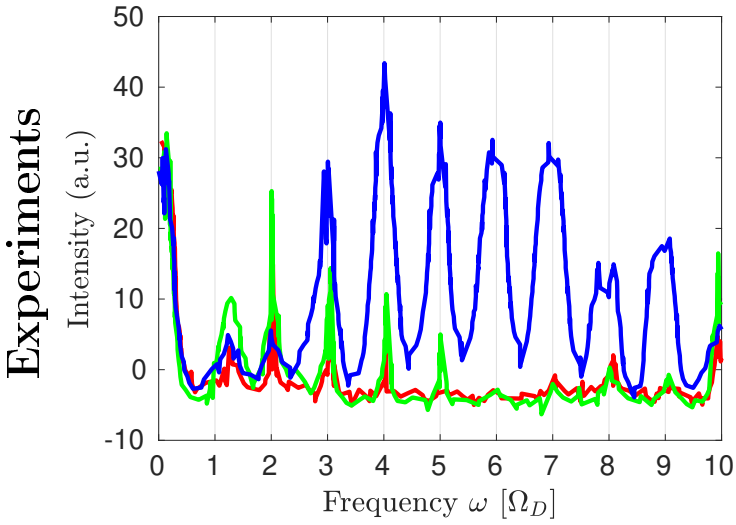

Observed LHD ICE power spectra, re-plotting Fig. 2 for cyclotron harmonics $\ell \leq 10$. The blue trace corresponds to LHD plasma 138433 ($v_{NBI}/V_A = 0.60$), the green trace to LHD plasma 138438 ($v_{NBI}/V_A = 0.44$) and the red trace to LHD plasma 138439 ($v_{NBI}/V_A = 0.36$).

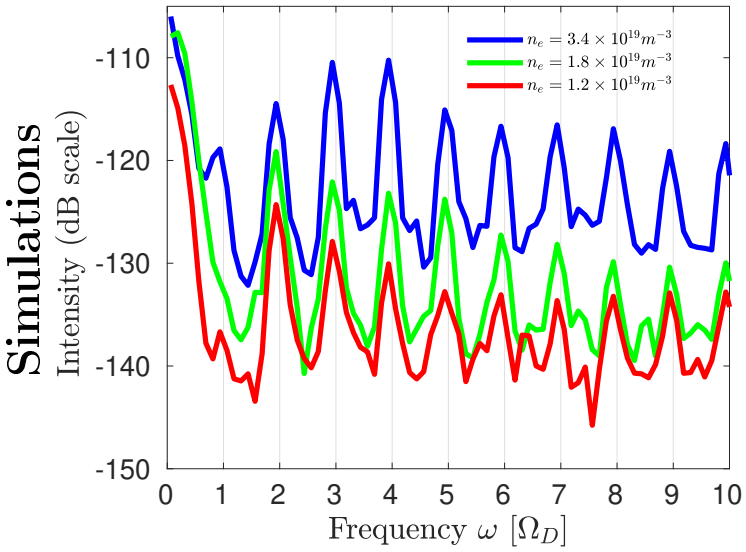

Corresponding simulated ICE power spectra, obtained from our PIC-hybrid computations by averaging the power of the z-component of the perturbed magnetic field between $t = \tau_D$ and $t = 9\tau_D$.

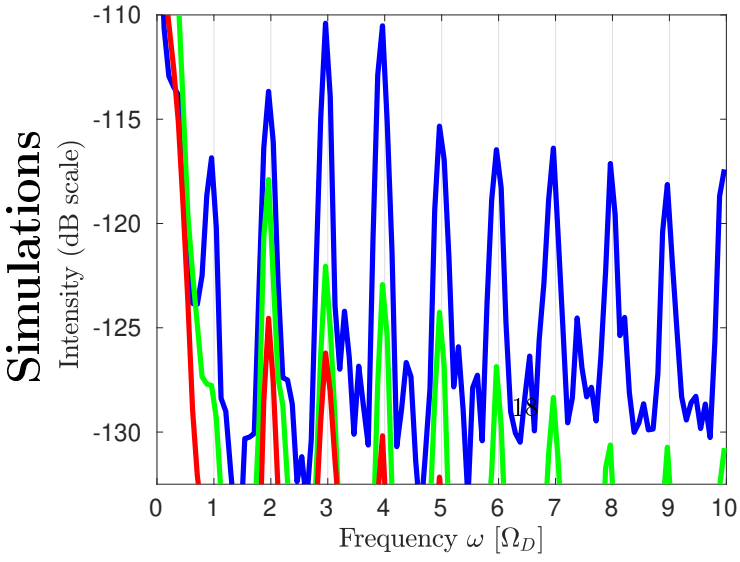

Simulated spectra from the middle panel, to which a conjectural instrumental detectability threshold at -133 dB has been applied.

Figure 6: Experimental and simulated power spectra.

these bands is approximately centered on a line which satisfies $\omega/k = v_{NBI}$. This is represented by the dark line in each panel of Fig. 8, for which $(\omega/k)/V_A = v_{NBI}/V_A = 0.36$, 0.44 and 0.60 from top to bottom. The steepest yellow-red feature in Fig. 8 corresponds to the linear fast Alfvén dispersion relation $\omega = kV_A$ and incorporates significant noise energy. Figure 9 plots the time evolution of the change in the different components of particle and field energy density. It shows that, in these simulations, the NBI beam deuterons relax and saturate faster, releasing more energy to the excited fields and the bulk plasma, as the value of v_{NBI}/V_A increases towards unity.

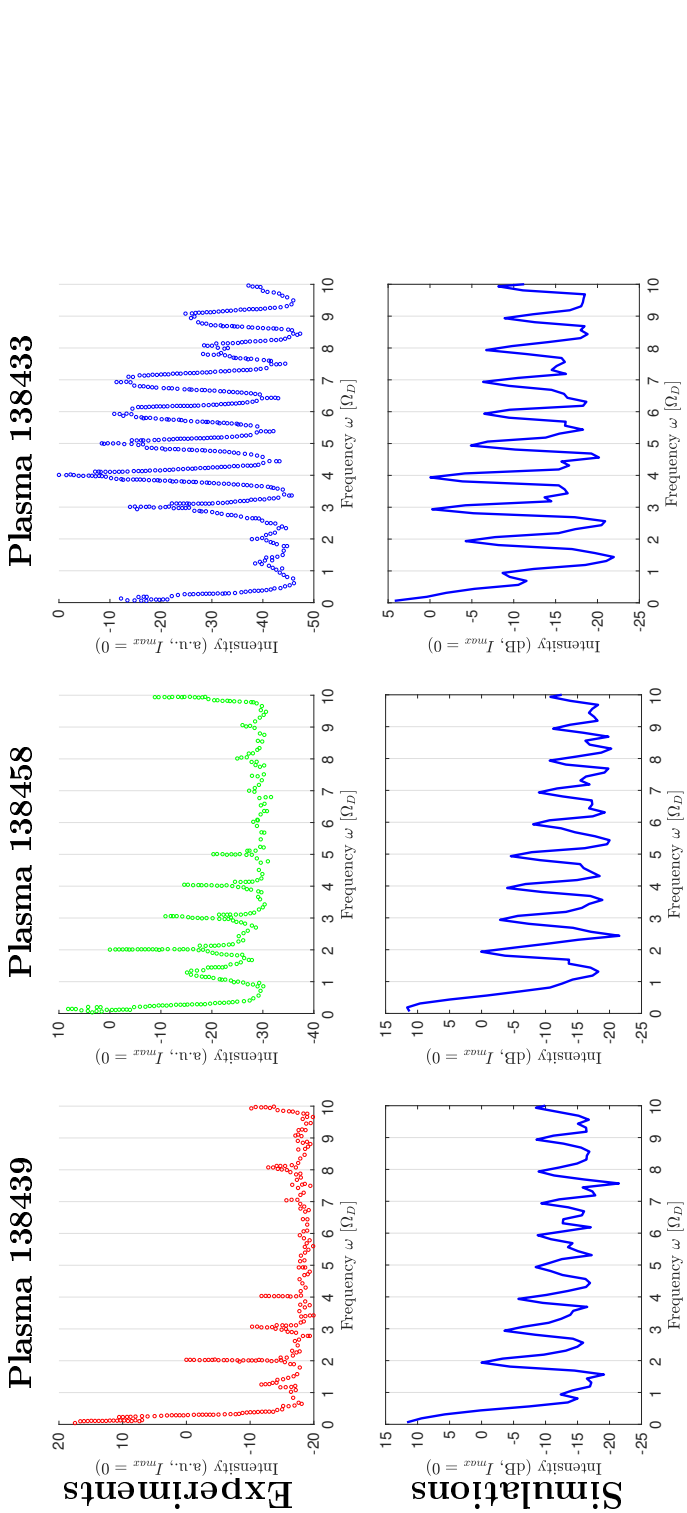

Figure 7: Red, green and blue circles: measured ICE power spectra from LHD plasmas 138439, 138458 at $t = 4.92$sec and 138433 at $t = 5.25$sec. Blue traces: corresponding simulated power spectra of the z-component of the perturbed magnetic field, averaged between $t = \tau_D$ and $t = 9\tau_D$. The power spectra are vertically offset in comparison to Fig. 6 such that the cyclotron harmonic with largest amplitude, respectively 2, 2 and 4 for LHD plasmas 138439, 138458 and 138433, has zero ordinate.

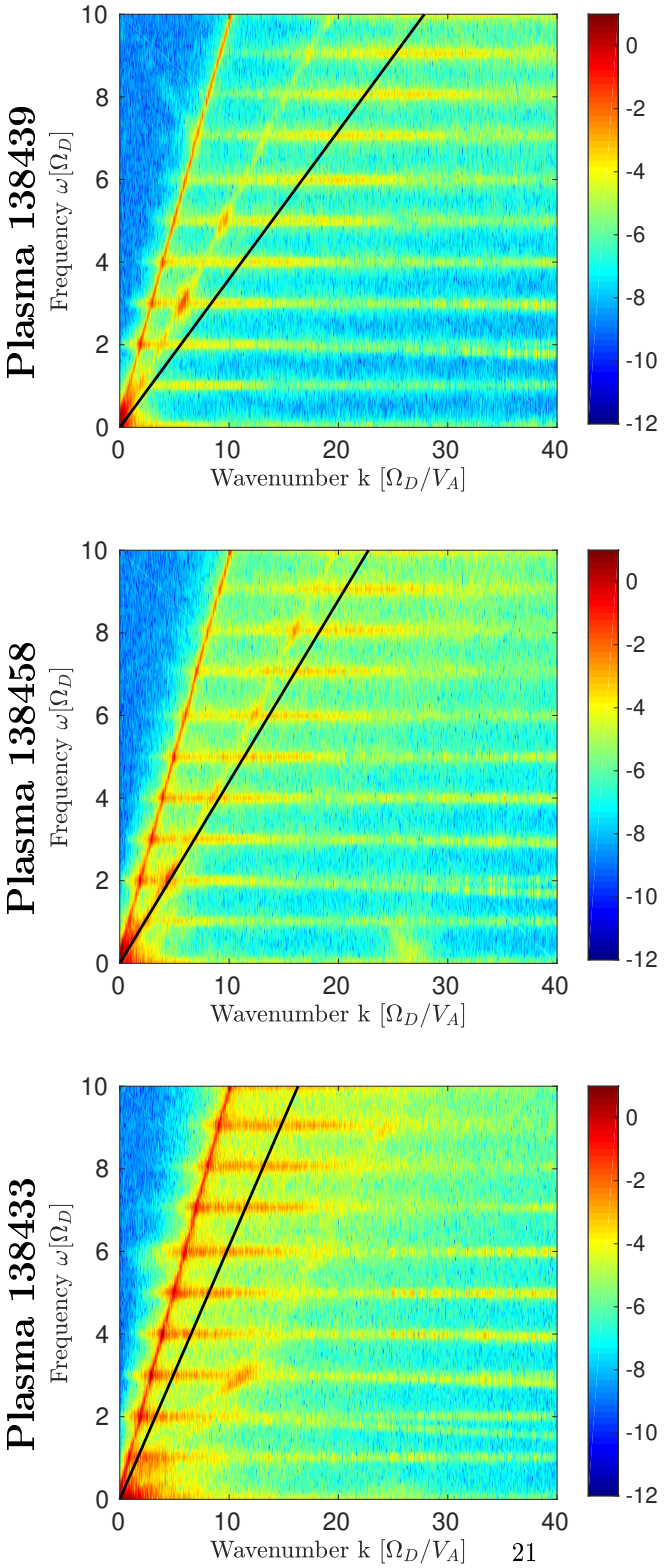

Figure 8: Spatiotemporal Fourier transform of the fluctuating part the z-component of the magnetic field, averaged over the entire simulation and plotted on a $\log_{10}$ scale for the three cases. The concentration of excited wave amplitude in (ω, k) space lies on horizontal bands at successive cyclotron harmonics, and each of these bands is approximately centered on a line which satisfies $\omega/k = v_{NBI}$. This is represented by the dark line in each panel, characterised by $(\omega/k)/V_A = v_{NBI}/V_A = 0.36$, 0.44 and 0.60 from left to right. The steepest yellow-red feature corresponds to the linear fast Alfvén dispersion relation $\omega = kV_A$ and incorporates significant noise energy.

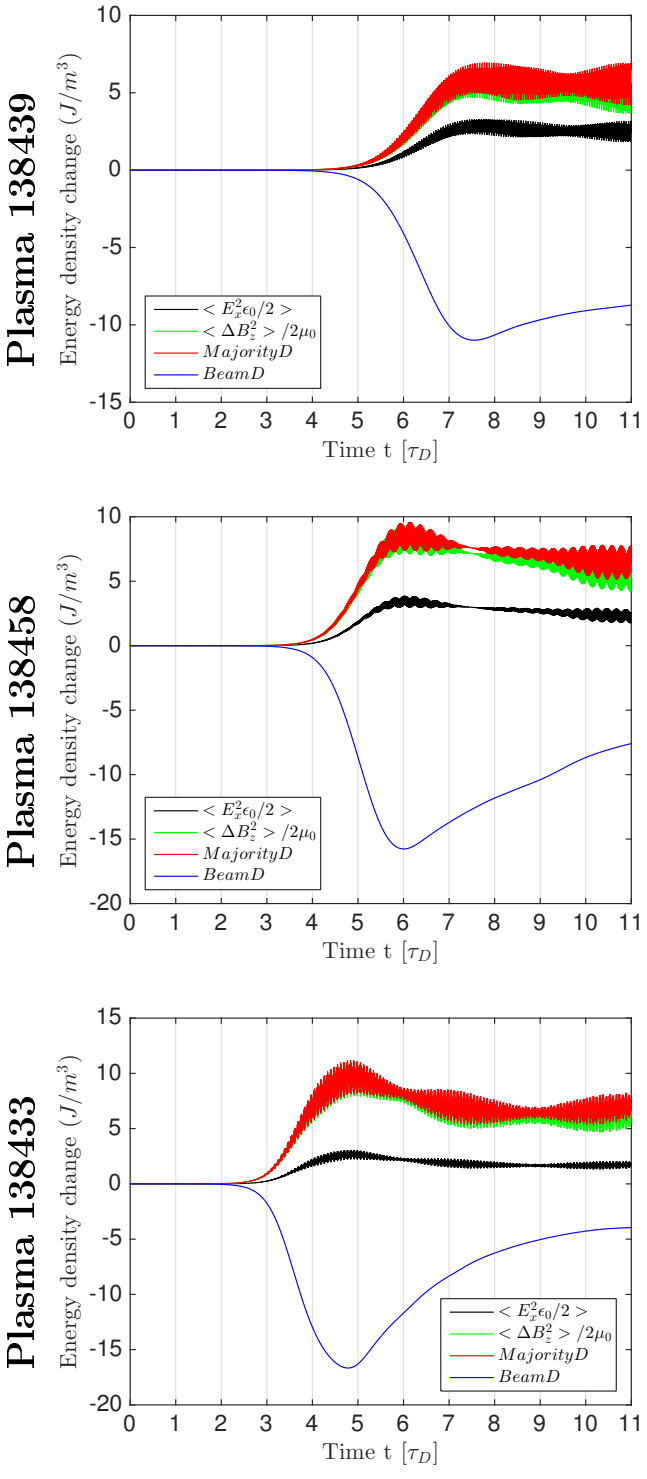

Figure 9: Time evolution of the change in the energy density of the different field and particle species: red, background deuterons; blue, NBI deuterons; green, z-component of the fluctuating part of the magnetic field; black, x-component of the electric field.

4 Conclusions

We are able to explain the physical origin of, and difference between, the ICE spectra obtained from three deuterium plasmas in LHD that differ primarily in their edge density. The collective instability of deuterons at about 67 keV originating from NBI #5, and relaxing under non the linear MCI in the outer midplane edge region is shown to be responsible for the ICE. An important consequence of the different edge densities across the three plasmas is that the ratio of v_{NBI}/V_A for freshly ionised NBI deuterons near their injection point changes while v_{NBI} is kept constant. The NBI deuterons are significantly sub-Alfvénic: $v_{NBI}/V_A = 0.36$, 0.44 and 0.61. Our PIC-hybrid computations of the collective relaxation of these NBI deuterons, evolving self-consistently with the thermal plasma and the excited electric and magnetic fields under the Maxwell-Lorentz equations, show good agreement with the LHD ICE observations. In particular, as the value of v_{NBI}/V_A increases, the number of cyclotron harmonic peaks in the simulated ICE spectra increases, along with their amplitude. These results are consistent with our recent comparison of ICE from super-Alfvénic and sub-Alfvénic NBI proton populations in LHD [18]. They also appear broadly consistent with the results of earlier ICE experiments carried out in TFTR, involving gas puffing [36, 37].

5 Acknowledgments

This work has been carried out within the framework of the EUROfusion Consortium and has received funding from the Euratom research and training programme 2014-2018 and 2019-2020 under grant agreement No 633053. The work received support from the RCUK Energy Programme [grant number EP/T012250/1], NIFS budget NIFS15KLPF045 and from NRF Korea grant no. 2014M1A7A1A03029881. The views and opinions expressed herein do not necessarily reflect those of the European Commission. ROD acknowledges the hospitality of Kyushu University. BCGR acknowledges helpful discussion with Dr. Carbajal-Gomez.

References

[1] Kenji Saito, Hiroe Igami, Mieko Toida, Tsuyoshi Akiyama, Shuji Kamio, Ryosuke Seki, LHD Experiment Group, et al. RF wave detection with high-frequency magnetic probes in LHD. *Plasma and Fusion Research*, 13:3402043–3402043, 2018.

[2] Shekar G. Thatipamula, G.S. Yun, J. Leem, Hyeon Keo Park, K.W. Kim, T. Akiyama, and S.G. Lee. Dynamic spectra of radio frequency bursts associated with edge-localized modes. *Plasma Physics and Controlled Fusion*, 58(6):065003, 2016.

[3] B. Chapman, R.O. Dendy, K.G. McClements, S.C. Chapman, G.S. Yun, S.G. Thatipamula, and M.H. Kim. Sub-microsecond temporal evolu-

tion of edge density during edge localized modes in KSTAR tokamak plasmas inferred from ion cyclotron emission. *Nuclear Fusion*, 57(12): 124004, 2017.

[4] TFR Equipe. High-power neutral injection and ion power balance in TFR. *Nuclear Fusion*, 18(9):1271, 1978.

[5] G.A. Cottrell, V.P. Bhatnagar, O. Da Costa, R.O. Dendy, J. Jacquinot, K.G. McClements, D.C. McCune, M.F.F. Nave, P. Smeulders, and D.F.H. Start. Ion cyclotron emission measurements during JET deuterium-tritium experiments. *Nuclear Fusion*, 33(9):1365, 1993. doi: 10.1088/0029-5515/33/9/I10. URL http://iopscience.iop.org/0029-5515/33/9/I10/.

[6] K.G. McClements, C. Hunt, R.O. Dendy, and G.A. Cottrell. Ion cyclotron emission from JET DT plasmas. *Physical Review Letters*, 82 (10):2099–2102, 1999. URL http://0-journals.aps.org.pugwash.lib.warwick.ac.uk/prl/pdf/10.1103/PhysRevLett.82.2099.

[7] R.O. Dendy, K.G. McClements, C.N. Lashmore-Davies, G.A. Cottrell, R. Majeski, and S. Cauffman. Ion cyclotron emission due to collective instability of fusion products and beam ions in TFTR and JET. *Nuclear Fusion*, 35(12):1733, 1995.

[8] Benjamin Chapman, Richard O. Dendy, Sandra C. Chapman, Kenneth G. McClements, Gunsu S. Yun, Shekar Goud Thatipamula, and Minho Kim. Nonlinear wave interactions generate high-harmonic cy-

clotron emission from fusion-born protons during a KSTAR ELM crash. *Nuclear Fusion*, 58(9):096027, 2018.

[9] B. Chapman, R.O. Dendy, S.C. Chapman, K.G. McClements, G.S. Yun, S.G. Thatipamula, and M.H. Kim. Interpretation of suprathermal emission at deuteron cyclotron harmonics from deuterium plasmas heated by neutral beam injection in the KSTAR tokamak. *Nuclear Fusion*, 59 (10):106021, 2019.

[10] KE Thome, DC Pace, RI Pinsker, MA Van Zeeland, WW Heidbrink, and ME Austin. Central ion cyclotron emission in the DIII-D tokamak. *Nuclear Fusion*, 59(8):086011, 2019.

[11] R Ochoukov, V Bobkov, B Chapman, R Dendy, M Dunne, H Faugel, M García-Muñoz, B Geiger, P Hennequin, KG McClements, et al. Observations of core ion cyclotron emission on ASDEX-Upgrade tokamak. *Review of Scientific Instruments*, 89(10):10J101, 2018.

[12] R Ochoukov, R Bilato, V Bobkov, B Chapman, SC Chapman, RO Dendy, M Dunne, H Faugel, M García-Muñoz, B Geiger, et al. Core plasma ion cyclotron emission driven by fusion-born ions. *Nuclear Fusion*, 59(1):014001, 2018.

[13] R Ochoukov, KG McClements, R Bilato, V Bobkov, B Chapman, SC Chapman, RO Dendy, M Dreval, H Faugel, J-M Noterdaeme, et al. Interpretation of core ion cyclotron emission driven by sub-Alfvénic

beam-injected ions via magnetoacoustic cyclotron instability. *Nuclear Fusion*, 59(8):086032, 2019.

[14] LG Askinazi, AA Belokurov, DB Gin, VA Kornev, SV Lebedev, AE Shevelev, AS Tukachinsky, and NA Zhubr. Ion cyclotron emission in NBI-heated plasmas in the TUMAN-3M tokamak. *Nuclear Fusion*, 58(8):082003, 2018.

[15] LN Liu, XJ Zhang, YB Zhu, CM Qin, YP Zhao, S Yuan, YZ Mao, MH Li, Y Chen, J Cheng, et al. Ion cyclotron emission diagnostic system on the experimental advanced superconducting tokamak and first detection of energetic-particle-driven radiation. *Review of Scientific Instruments*, 90(6):063504, 2019.

[16] Kenji Saito, H. Kasahara, T. Seki, R. Kumazawa, Takashi Mutoh, Tsuguhiro Watanabe, Fujio Shimpo, Goro Nomura, Masaki Osakabe, M Ichimura, et al. Measurement of ion cyclotron emissions by use of ICRF heating antennas in LHD. *Fusion Engineering and Design*, 84 (7):1676–1679, 2009.

[17] Kenji Saito, Ryuhei Kumazawa, Tetsuo Seki, Hiroshi Kasahara, Goro Nomura, Fujio Shimpo, Hiroe Igami, Mitsutaka Isobe, Kunihiro Ogawa, Kazuo Toi, et al. Measurement of ion cyclotron emissions by using high-frequency magnetic probes in the lhd. *Plasma Science and Technology*, 15(3):209, 2013.

[18] BCG Reman, RO Dendy, T Akiyama, SC Chapman, JWS Cook,

H Igami, S Inagaki, K Saito, and GS Yun. Interpreting observations of ion cyclotron emission from large helical device plasmas with beam-injected ion populations. *Nuclear Fusion*, 59(9):096013, 2019.

[19] Shekar G Thatipamula, MH Kim, J Kim, JH Kim, and GS Yun. Radio frequency emissions driven by energetic ions from neutral beam in kstar low confinement mode plasma. *Plasma Physics and Controlled Fusion*, 62(3):035004, 2020.

[20] Kenneth G McClements, Alexandra Brisset, Benjamin Chapman, Sandra C Chapman, Richard O Dendy, Philippe Jacquet, Vasily Kiptily, Mervi Mantsinen, and Bernard CG Reman. Observations and modelling of ion cyclotron emission observed in JET plasmas using a sub-harmonic arc detection system during ion cyclotron resonance heating. *Nuclear Fusion*, 58(9):096020, 2018.

[21] KE Thome, DC Pace, RI Pinsker, O Meneghini, CA del Castillo, and Y Zhu. Radio frequency measurements of energetic-particle-driven emission using the ion cyclotron emission diagnostic on the DIII-D tokamak. *Review of Scientific Instruments*, 89(10):10I102, 2018.

[22] V.S. Belikov and Ya. I. Kolesnichenko. *Soviet Physics Technical Physics*, 20:1146, 1976.

[23] R.O. Dendy, Chris N. Lashmore Davies, and K.F. Kam. A possible excitation mechanism for observed superthermal ion cyclotron emission from tokamak plasmas. *Physics of Fluids B:*

Plasma Physics (1989-1993), 4(12):3996–4006, 1992. doi: 10.1063/1.860304. URL http://scitation.aip.org/content/aip/journal/pofb/4/12/10.1063/1.860304.

[24] R. O. Dendy, C.N. Lashmore Davies, and K. F. Kam. The magnetoacoustic cyclotron instability of an extended shell distribution of energetic ions. *Physics of Fluids B: Plasma Physics (1989-1993)*, 5(7): 1937–1944, 1993.

[25] R.O. Dendy, C.N. Lashmore-Davies, K.G. McClements, and G.A. Cottrell. The excitation of obliquely propagating fast Alfvén waves at fusion ion cyclotron harmonics. *Physics of Plasmas*, 1(6):1918–1928, 1994. doi: 10.1063/1.870647. URL http://dx.doi.org/10.1063/1.870647.

[26] R.O. Dendy, K.G. McClements, C.N. Lashmore-Davies, R. Majeski, and S. Cauffman. A mechanism for beam-driven excitation of ion cyclotron harmonic waves in the Tokamak Fusion Test Reactor. *Physics of Plasmas*, 1(10):3407–3413, 1994.

[27] J.W.S. Cook, R. O. Dendy, and S.C. Chapman. Particle-in-cell simulations of the magnetoacoustic cyclotron instability of fusion-born alpha particles in tokamak plasmas. *Plasma Physics and Controlled Fusion*, 55(6):065003, 2013.

[28] L. Carbajal, R. O. Dendy, S.C. Chapman, and J.W.S. Cook. Linear and nonlinear physics of the magnetoacoustic cyclotron instability of fusion

born-ions in relation to ion cyclotron emission. *Physics of Plasmas*, 21 (1):012106, 2014.

[29] J.W.S. Cook, R.O. Dendy, and S.C. Chapman. Stimulated emission of fast Alfvén waves within magnetically confined fusion plasmas. *Physical Review Letters*, 118(18):185001, 2017.

[30] L. Carbajal, R.O. Dendy, S.C. Chapman, and J.W.S. Cook. Quantifying fusion born ion populations in magnetically confined plasmas using ion cyclotron emission. *Physical Review Letters*, 118(10):105001, 2017.

[31] T.D. Arber, Keith Bennett, C.S. Brady, A. Lawrence-Douglas, M.G. Ramsay, N.J. Sircombe, P. Gillies, R.G. Evans, Holger Schmitz, A.R. Bell, et al. Contemporary particle-in-cell approach to laser-plasma modelling. *Plasma Physics and Controlled Fusion*, 57(11):113001, 2015.

[32] G Yun and T Akiyama. Fast RF Spectrometer System on LHD. *Annual Report of National Institute for Fusion Science*, page 46, 2012.

[33] G Yun and T Akiyama. Fast RF Spectrometer System on LHD. *Annual Report of National Institute for Fusion Science*, page 53, 2013.

[34] G Yun and T Akiyama. Fast RF Spectrometer System on LHD. *Annual Report of National Institute for Fusion Science*, page 58, 2014.

[35] Minho Kim, Shekar Goud Thatipamula, Jayhyun Kim, Minjun J Choi, Jaehyun Lee, Woochang Lee, Minwoo Kim, Youngdae Yoon, and

Gunsu S Yun. Intense whistler-frequency emissions at the pedestal collapse in KSTAR H-mode plasmas. *Nuclear Fusion*, 60:126021, 2020.

[36] S. Cauffman and R. Majeski. Ion cyclotron emission on the Tokamak Fusion Fest Reactor. *Review of Scientific Instruments*, 66(1):817–819, 1995.

[37] S. Cauffman, R. Majeski, K.G. McClements, and R.O. Dendy. Alfvénic behaviour of alpha particle driven ion cyclotron emission in TFTR. *Nuclear Fusion*, 35(12):1597, 1995.

[38] D.W. Hewett. Low-frequency electromagnetic (Darwin) applications in plasma simulation. *Computer Physics Communications*, 84(1):243 – 277, 1994. ISSN 0010-4655. doi: https://doi.org/10.1016/0010-4655(94)90214-3. URL http://www.sciencedirect.com/science/article/pii/0010465594902143.

[39] D Winske and N Omidi. A nonspecialist's guide to kinetic simulations of space plasmas. *Journal of Geophysical Research: Space Physics*, 101 (A8):17287–17303, 1996.

[40] Charles K Birdsall and A Bruce Langdon. *Plasma physics via computer simulation*. CRC press, 2004.

[41] R.D. Sydora. Low-noise electromagnetic and relativistic particle-in-cell plasma simulation models. *Journal of Computational and Applied Mathematics*, 109(1):243–259, 1999.

[42] Rep Kubo. The fluctuation-dissipation theorem. *Reports on Progress in Physics*, 29(1):255, 1966.

A Appendix

We have checked the noise level of our results by running PIC-hybrid simulations without an energetic minority population, retaining only the deuterium thermal background plasma, and with all other parameters kept equal, for each of three plasmas. The top panel of Fig. 10 displays: the power spectra for computations that include both the NBI and thermal deuterons, shown by continuous lines; and the spectra obtained from the simulations that retain only the thermal deuterium plasma, shown by the dashed curves. The spectral peaks in the latter case result from the concentration of noise energy at normal modes - in this case, cyclotron harmonic waves supported by the thermal plasma - in line with the fluctuation dissipation theorem [42]. From the bottom panel of Fig. 10, we see that the fundamental computational noise level is similar in all our simulations, at -145dB, although slightly higher for the simulation of LHD plasma 138433.

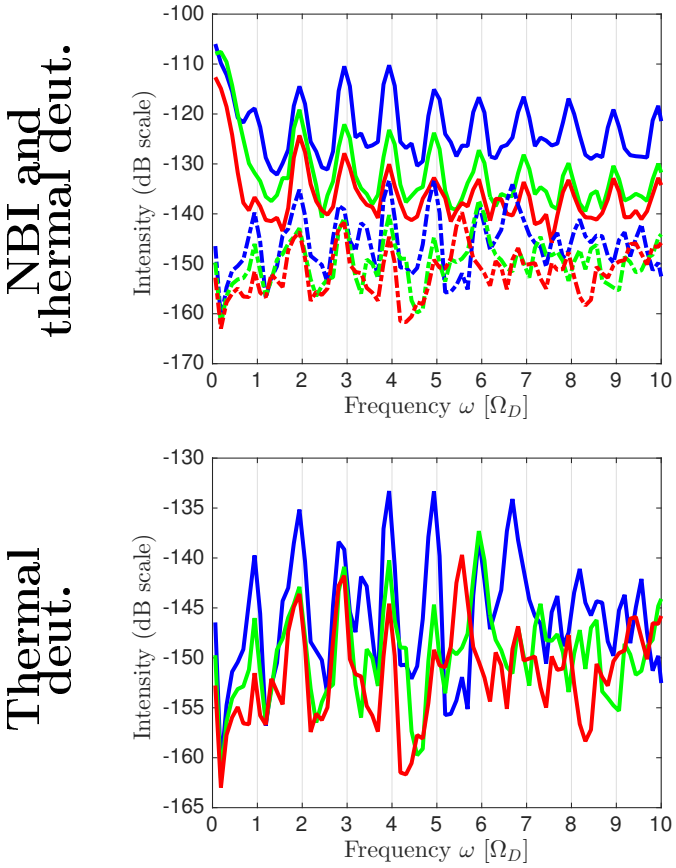

Superimposed simulated ICE power spectra. The blue, green and red traces respectively correspond to LHD plasma parameters 138433, 138458 and 138439. The associated dashed lines are the background noise level in each of these simulations.

Background noise level for simulated LHD plasma parameters 138433 (blue), 138458 (green) and 138439 (red).

Figure 10: Quantifying the effect of noise on spectral characteristics in our PIC-hybrid simulations. Power spectra from simulations that contain both NBI and thermal deuterons are shown as solid traces in the top panel. Spectra from simulations that contain thermal deuterons only, with no energetic minority NBI deuterons, are shown as dashed lines in the top panel, and are displayed separately in the bottom panel. In both panels, the blue, green and red traces respectively correspond to LHD plasma parameters at the ICE location for plasmas 138433 ($v_{NBI}/V_A = 0.60$), 138458 ($v_{NBI}/V_A = 0.44$) and 138439 ($v_{NBI}/V_A = 0.36$). Spectral peaks in the absence of NBI deuterons reflect the concentration of noise energy at normal modes as a consequence of the fluctuation-dissipation theorem [42] and the effect of integrating over wavenumber space.